Improved Whale Optimization Algorithm with Deep Learning-Driven Retinal Fundus Image Grading and Retrieval

Syed Ibrahim Syed Mahamood Shazuli
Department of Computer and Information Sciences, Annamalai University, India
syedshazuli@yahoo.co.in

Arunachalam Saravanan
Department of Computer and Information Sciences, Annamalai University, India
vmahafx@gmail.com

Received: 8 June 2023 | Revised: 22 June 2023 | Accepted: 29 June 2023

 DOI: https://doi.org/10.48084/etasr.6111

ABSTRACT

Several Deep Learning (DL) and medical image Machine Learning (ML) methods have been investigated for efficient data representations of medical images, such as image classification, Content-Based Image Retrieval (CBIR), and image segmentation. CBIR helps medical professionals make decisions by retrieving similar cases and images from electronic medical image databases. CBIR needs expressive data representations for similar image identification and knowledge discovery in massive medical image databases explored by distinct algorithmic methods. In this study, an Improved Whale Optimization Algorithm with Deep Learning-Driven Retinal Fundus Image Grading and Retrieval (IWOADL-RFIGR) approach was developed. The presented IWOADL-RFIGR method mainly focused on retrieving and classifying retinal fundus images. The proposed IWOADL-RFIGR method used the Bilateral Filtering (BF) method to preprocess the retinal images, a lightweight Convolutional Neural Network (CNN) based on scratch learning with Euclidean distance-based similarity measurement for image retrieval, and the Least Square Support Vector Machine (LS-SVM) model for image classification. Finally, the IWOA was used as a hyperparameter optimization technique to improve overall performance. The experimental validation of the IWOADL-RFIGR model on a benchmark dataset exhibited better performance than other models.

Keywords-retinal fundus images; image retrieval; image classification; deep learning; parameter tuning

I. INTRODUCTION

Data retrieval plays an important role in the evolution of technology in the current technological scenario with several databases [1]. CIBR is one of the most common image retrieval methods, which is applied in various domains, such as military applications, medical image analysis, historical research, and many more. Effective data representation and feature extraction are the main elements of successful medical imaging tasks [2]. Researchers generally adopt medical field knowledge and ask for annotations from medical experts. For example, conventional image processing methods, such as filters or edge detection methods, are used to extract clinically related spatial features from images obtained using distinct image modalities [3]. All significant areas of the internal eye constitute the fundus area, which can be identified just opposite the eye lens. The fundus area contains the posterior pole, fovea, retina, optic disc, macula, and blood vessels present in the eye [4]. An ophthalmoscope is used to analyze the fundus area of the eye. The analysis of the fundus area is performed with the help of a fundus high-resolution camera [5], which operates on the same principle as the ophthalmoscope. Numerous medical conditions of the eye, such as cotton wool spots, exudates, constrictions and abnormalities in blood vessels, hemorrhages, etc., can be monitored using images acquired from a fundus camera [6].

Over the years, DL has been implemented in several domains, including medical image analysis [7]. DL may recognize features precisely from input data for segmentation or classification and commonly outpaces every conventional image analysis method. DL methods do not need to derive handcrafted features, whereas they needed broad data for training purposes [8]. On the contrary, ML methods need the extraction of handcrafted features but do not require large data for training purposes. In DR recognition, ML methods have to derive the vessel initially, following the DR lesions' extraction factors for classification purposes. DL applications cover image detection, segmentation, retrieval, registration, and classification. Convolutional Neural Networks (CNNs) are a commonly used DL method that has a very high potential for image analysis [9]. There is a substantial amount of effort in

automating DR image classification through DL to help eye specialists identify diseases at their initial levels. On the other hand, many of these efforts focus on recognizing DR rather than finding several DR levels [10]. Additionally, limited efforts were made to locate and classify every DR lesion type, which is highly useful in practice as ophthalmologists could assess the severity of DR and observe its development related to the appearance of such lesions.

This study developed the Improved Whale Optimization Algorithm with Deep Learning-Driven Retinal Fundus Image Grading and Retrieval (IWOADL-RFIGR) method. The proposed method used the Bilateral Filtering (BF) approach to preprocess retinal images, lightweight CNN based on scratch learning with Euclidean distance-based similarity measurement for image retrieval, and the Least Square Support Vector Machine (LS-SVM) model for image classification. Finally, the IWOA was used as a hyperparameter optimization method to improve overall performance. The proposed method was experimentally validated on a benchmark dataset.

II. RELATED WORKS

In [11], an optimal deep CNN was developed for RF image classification, using the U-Net approach for image segmentation and allowing the infested area to be properly identified. The EfficientNet feature extraction algorithm was used to create a feature vector. Finally, the Mayfly Optimization with KELM (MFO-KELM) method was executed for classification. In [12], a novel AI with an Optimal DCNN (AI-ODCNN) system was proposed for RFIC, using Gaussian blur noise removal and CLAHE-based contrast advancement to preprocess the RFI. In addition, DCNN with RMSProp Optimization was used for RFIC. In [13], a new two-step optical disk location and glaucoma diagnosis network was presented. In the primary step, a visual saliency mapping was integrated with a shallow CNN to locate effectual OD in the retinal image. TL-based pre-training approaches were used for glaucoma analysis during the secondary step. TL-based techniques, such as VGG-Net, Alex-Net, and Res-Net, were integrated with the saliency maps. In [14], a new multimodel DL network called G-EyeNet was presented to detect glaucoma in RFIs. G-EyeNet contained a deep convolutional Auto-Encoder (AE) and a classic CNN shared the encoded structure. The multi-model network had combined optimizations to minimize either image reconstruction or classifier error, depending on the multitask learning system.

In [15], a two-stage structure was investigated to identify and localize the optic disc and later classify it as glaucomatous or healthy. The primary phase depended on Regions with CNN (RCNN) and was responsible for localizing and extracting OD in RFI, but the secondary phase utilized DCNN to classify the extracted disc. So, a ruling-related semiautomated ground truth generating system was established, which offered essential annotations to train RCNN-based methods to automated disc localization. In [16], a new LSTM-based model was presented to exploit the sequence dependency of 1-D feature signal extraction in MAs and support its classifier from color fundus images. This method was trained to use 1-D intensity-based signals created in several patches of preprocessed fundus images.

III. THE PROPOSED METHOD

This study developed the innovative IWOADL-RFIGR method to retrieve and classify retinal fundus images. The proposed process consisted of different sub-processes, namely BF-based preprocessing, feature extraction, similarity measurement, classifying LS-SVM, and the IWOA tuning process. Figure 1 describes the comprehensive procedure of the IWOADL-RFIGR method.

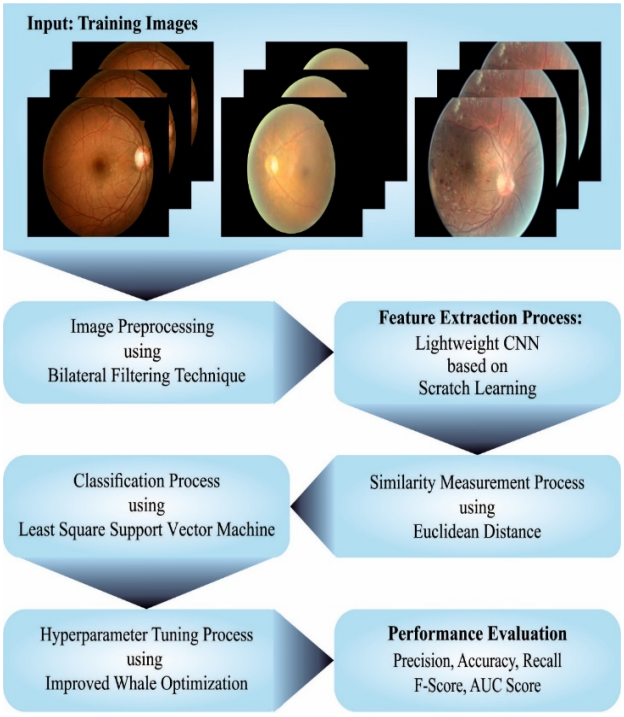

Fig. 1. Comprehensive procedure of the IWOADL-RFIGR method.

A. Image Preprocessing

In the first phase, the proposed IWOADL-RFIGR method used the BF approach to preprocess the retinal images. The BF method is an edge-preserving, non-serial, and noise-reducing smooth filtering method, including two properties [17]. The process guarantees the conservation of sharp edges along with noise reduction. A BF of an image $f(x)$ can be determined as follows:

$$h(z) = k_r^{-1}(z) \int_{\Omega} f(\xi) c(\xi, z) s\big(f(\xi), f(z)\big) d\xi \quad (1)$$

with the normalizing:

$$k(z) = \int_{\Omega} c(\xi, z) s\big(f(\xi), f(z)\big) d\xi \quad (2)$$

where $c(\xi, z)$ measures the geometric proximity between the local regions centered on every point ξ and its adjacent pixel z, and $s(f(\xi), f(z))$ is an unbiased function that measures the photometric similarities between the central pixel z and its neighboring pixel ξ. The scientific representations of s and c in the above equations are determined as:

$$c(\xi, z) = exp\left(-\frac{1}{2}\left(\frac{\|\xi - z\|}{\sigma_d}\right)^2\right) \quad (3)$$

$$s(\xi, z) = exp(-\frac{1}{2}\left(\frac{\|f(\xi)-f(z)\|}{\sigma_r}\right)^2) \quad (4)$$

B. Image Retrieval Process

For image retrieval, the IWOADL-RFIGR method uses the lightweight CNN based on scratch learning with Euclidean distance-based similarity measurement. A well-generalized lightweight CNN with Scratch Learning (SL) was presented in [18]. This method integrates standard and depthwise separable convolution with skip connections and embeds the block of edge detection to improve the recognition ability. There are two typical convolution layers in the initial block of the method, having sizes of 3×3 and 1×1. It uses a bias regularizer of 0.01, a six-dilation rate, and a regularizer of 0.01. A nonlinear activation function and batch normalization (ReLU) was applied in the initial block to restrain the number of parameters and, simultaneously, to reinforce the network to offer a short description of the input images. Besides the typical convolutional block, there are six successive depthwise separable blocks that have both the dilation rate and depth multiplier parameters set at 6. In addition to the six blocks of the depthwise convolution layer, the sequence continues with the edge attention block. The real-time application of dropout was set at 0.25 to prevent overfitting after blocks 4, 5, and 6. The conventional model of max-pooling or average layers was not used due to the characteristics of spatial-dimensionality reduction. However, 1×1 convolution was applied in each block to reduce channel dimension. ReLU was used after every block. The padding within the typical and depthwise convolution blocks was employed as "the same". At the same time, the depth-multiplayer rate was noted as six in the initial block of a typical convolutional layer. The last stage of the architecture consists of *k*-way sigmoid activation to generate distribution through *k*-class labeling in edge attention blocks to decide the concluding forecasting. After feature extraction, image retrieval takes place via Euclidean distance. The Euclidean distance between two points in Euclidean space is the length of the line segment between them. This was computed from the Cartesian coordinates of the points using the Pythagorean theorem.

C. Image Classification Process

The IWOADL-RFIGR method uses IWOA with the LS-SVM model for image classification. LS-SVM is an ML technique established in typical SVM [19]. SVMs are primarily used for classifier problems and non-linear function evaluation. Many researchers stated that SVM depends on regression systems, such as Support Vector Regression (SVR), for resolving particular modeling like predictive drives. Usually, the SVR network is established as:

$$f(x) = \langle \omega, \varphi(x) \rangle + b \quad (5)$$

where χ denotes the inputted database, $\langle \ \rangle$ represents the dot product, and ω, b, and $\varphi(x)$ imply the weight vectors, bias, and non-linear functions that map input spacing to higher dimension factor spacing. To make N count of data instances from the SVM, the optimized problem was determined as:

$$\min \frac{1}{2}\|\omega\|^2 + C\sum_{k=1}^{N}(\xi_k + \xi_k^*) S.T. \begin{cases} y_k - \langle \omega, \varphi(x_k) \rangle - b \le \varepsilon + \xi, e \\ \langle \omega, \varphi(x_k) \rangle + b - y_k \le \varepsilon + \xi_e^* \\ \xi \ \xi_e^* \ge 0 \end{cases} \quad (6)$$

where ξ and ε denote the insensitive loss functioning and the slack variable, respectively. SVMs can model problems with higher-dimension input spaces and have been effectively used to model many hydrological procedures. At this point, the original term SVM can be used for either the predictive or classifier methods. However, due to the SVM's vital constrained optimized programming, it can undergo higher computation costs in modeling complicated phenomena. To resolve this problem, the LS-SVM method was used. In this study, the sum squared error and equality constraint of the cost function was applied for the training method as:

$$\min \frac{1}{2}\|\omega\|^2 + \frac{1}{2}\gamma\sum_{e=1}^{N} e_k^2 \, S.T. \begin{cases} \langle \omega, \varphi(x_k) \rangle + b + e_k \\ \gamma \ge 0 \\ k = 1, \dots, N \le \varepsilon + \xi_{1e} \end{cases} \quad (7)$$

where e_k refers to the error variable, and γ denotes a normalization constant. LS-SVM shortens the model process of SVM so that the resolution is delineated via the Karush-Kuhn-Tucker linear method. The presented linear method is merely resolved using an iterative method, including gradient-based optimization methodology. The predicted value (output) of the LS-SVM is evaluated by the following equation:

$$y(k) = \sum_{k=1}^{\Sigma} \alpha_k \, K(x, x_k) + b \quad (8)$$

where $K()$ signifies the kernel function considered an RBF for the kernel function as:

$$K(x, x_k) = \exp\left(-\frac{(x-x_k)^T(x-x_k)}{2\sigma^2}\right) \quad (9)$$

where σ defines the width of the kernel function.

The use of IWOA optimally chooses the parameters related to the LS-SVM model. It has a certain capability to escape from the local optima, a faster operational speed, and a simple adjustment parameter [20]. However, the algorithm exploits an arbitrary method for exploration, and overreliance on the random limit search speed of the model, convergence accuracy, and the speed of WOA increased. Furthermore, because of the constraint of the B coefficient vector, WOA loses its capability to escape from local optima once the iteration number reaches half of the maximal iteration. Consequently, WOA has a distinct possibility of falling into local optima, which leads to improper predictive outcomes. To resolve the abovementioned problems, this study presents an improved WOA, using Levy flight that has the best capability for escaping from the local optima, a fast convergence speed, and high convergence precision. Levy flight searching is based on Levy dispersion, which is a random-wise manner of larger range jump and smaller range search, and it can be represented as follows:

$$X(t+1) = X^*(t) - BD_1 \quad (10)$$

where t represents the current iteration amount, B and M represent the coefficient vectors:

$$B = 2aLevy(\lambda) - a \quad (11)$$

$$M = 2r_2 \quad (12)$$

where 1 is the constant upgrade distance size, H is the vector of coefficient, $X^*(t)$ is the location vector of the present optimum resolution, $X(t)$) is the existing location vector of humpback whales, $Xrand(t)$ is the random location vector, τ_p is the distance between the prey and the whale populace, a represents the parameter that is reduced from two to zero, ε defines the spiral movement shaping, m is a random vector within [1, 1], and n is the probability parameter.

LWOA was used to resolve the optimization problems for TSVR. The LWOA is iteratively repeated to search for the concluding solution. In this study, the industrial trial dataset was normalized and used rapidly. Subsequently, the input variable was defined and nine input parameters were improved using the LWOA optimization. The population number was 30, the iteration number was 500, and the search range of the variable was [1, 1]. The initial iteration randomly generated 30 groups of the first solution, computed every set of resolutions fitness, and saved the set of resolutions with smaller fitness as a present optimum resolution for completing these iterations. Upon entering the following iteration, the position of 30 solutions was upgraded, and the set of solutions with lower fitness was related to the present optimum resolution to store the set of resolutions with the lowest fitness.

IV. RESULTS AND DISCUSSION

The performance evaluation of the IWOADL-RFIGR method was investigated using the DR Kaggle database [21] with 35126 samples and 5 class labels. Figure 2 shows some sample images and Figure 3 shows the sample retrieving outputs of the IWOADL-RFIGR method. The proposed method was simulated using Python 3.6.5 on an i5-8600K, GeForce 1050Ti 4GB, 250GB SSD, 16GB RAM, and 1TB HDD PC. The parameter settings were given as follows: learning rate: 0.01, dropout: 0.5, batch size: 5, epoch count: 50, and activation: ReLU. Figure 4 shows the confusion matrix of the IWOADL-RFIGR method. The results indicate that the IWOADL-RFIGR approach has a proficient classification of retinal fundus images.

Table I exhibits the comprehensive DR classifying outputs of the IWOADL-RFIGR method on 70:30 TR:TS of the dataset. The proposed method, with 70% TR, achieved average $accu_y$, $prec_n$, $reca_l$, F_{score}, and AUC_{score} of 99.69%, 97.53%, 98.40%, 97.96%, and 99.06%, respectively. Simultaneously, with 30% TS of the dataset, the IWOADL-RFIGR method achieved average $accu_y$, $prec_n$, $reca_l$, F_{score}, and AUC_{score} of 99.72%, 97.53%, 98.58%, 98.04%, and 99.16%, respectively. Table II demonstrates the respective DR classifying outputs of the proposed method on 80:20 TR:TS. On the 80% of the TR dataset, the proposed method achieved average $accu_y$, $prec_n$, $reca_l$, F_{score}, and AUC_{score} of 99.23%, 93.20%, 93.85%, 93.50%, and 96.58%, respectively. On the 20% of the TS dataset, the proposed method achieved average $accu_y$, $prec_n$, $reca_l$, F_{score}, and AUC_{score} of 99.33%, 93.10%, 95.52%, 94.25%, and 97.50%, respectively.

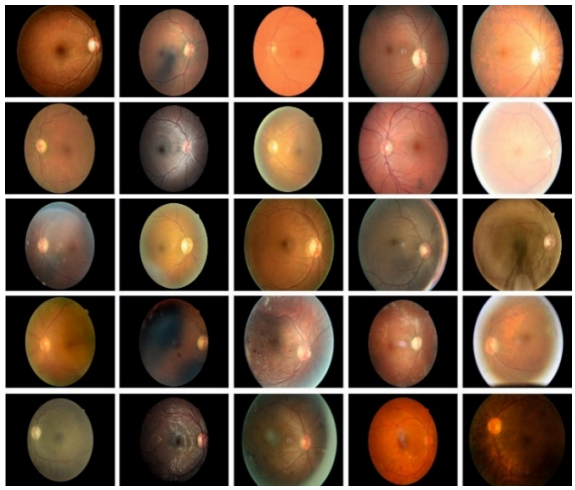

Fig. 2. Sample images.

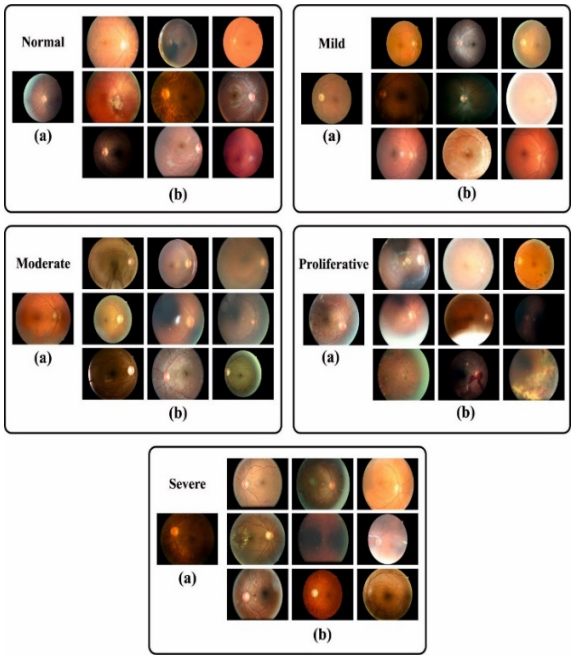

Fig. 3. (a) Query Images, (b) retrieved Images.

TABLE I. RESULTS EVALUATION OF IWOADL-RFIGR UNDER 70:30 TR:TS DATA

Labels	$accu_y$	$prec_n$	$reca_l$	F_{score}	AUC_{score}
Training Stage (70%)					
1st Class	99.36	99.70	99.43	99.56	99.29
2nd Class	99.70	97.72	98.00	97.86	98.92
3rd Class	99.70	98.68	99.32	99.00	99.54
4th Class	99.84	96.83	96.67	96.75	98.30
5th Class	99.86	94.74	98.58	96.62	99.23
Average	**99.69**	**97.53**	**98.40**	**97.96**	**99.06**
Testing Stage (30%)					
1st Class	99.44	99.75	99.48	99.62	99.40
2nd Class	99.75	98.25	98.25	98.25	99.06
3rd Class	99.70	98.70	99.31	99.00	99.54
4th Class	99.82	96.68	96.32	96.50	98.12
5th Class	99.87	94.27	99.53	96.83	99.70
Average	**99.72**	**97.53**	**98.58**	**98.04**	**99.16**

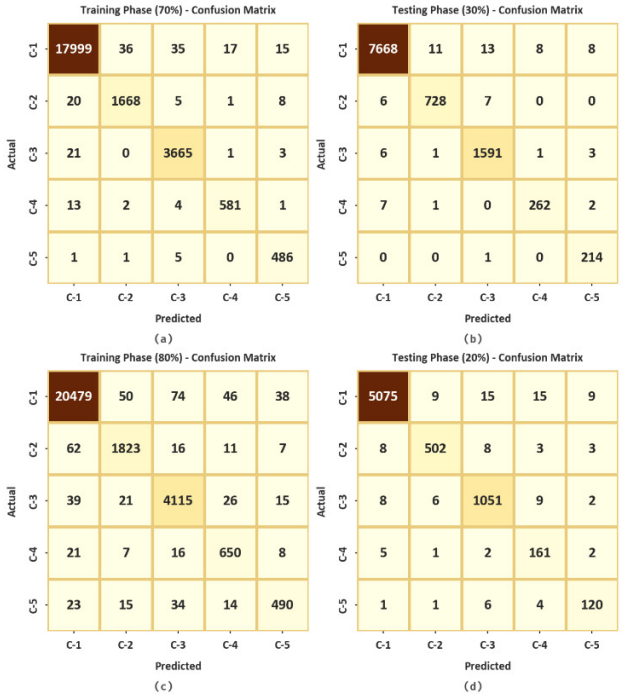

Fig. 4. Confusion matrix of IWOADL-RFIGR: (a)-(b): 70:30 TR and TS dataset, and (c)-(d): 80:20 TR and TS dataset.

TABLE II. RESULTS EVALUATION OF IWOADL-RFIGR UNDER 80:20 TR:TS DATA

Labels	$accu_y$	$prec_n$	$reca_l$	F_{score}	AUC_{score}
Training Stage (80%)					
1st Class	98.74	99.30	98.99	99.15	98.52
2nd Class	99.33	95.15	95.00	95.07	97.32
3rd Class	99.14	96.71	97.60	97.15	98.51
4th Class	99.47	87.01	92.59	89.72	96.12
5th Class	99.45	87.81	85.07	86.42	92.41
Average	**99.23**	**93.20**	**93.85**	**93.50**	**96.58**
Testing Stage (20%)					
1st Class	99.00	99.57	99.06	99.32	98.95
2nd Class	99.44	96.72	95.80	96.26	97.77
3rd Class	99.20	97.13	97.68	97.41	98.58
4th Class	99.42	83.85	94.15	88.71	96.85
5th Class	99.60	88.24	90.91	89.55	95.34
Average	**99.33**	**93.10**	**95.52**	**94.25**	**97.50**

TABLE III. ACCURACY EVALUATION OF IWOADL-RFIGR WITH CURRENT ALGORITHMS [22]

Method	$accu_y$
IWOADL-RFIGR	99.72
RFIRC-ODL	99.61
WFDLN	98.00
Alex-Net	89.50
Mobile-Net	92.90
Xception	92.80
ResNet-50	94.51

Table III shows an overall comparison of the proposed IWOADL-RFIGR with other methods, in terms of $accu_y$. The proposed method achieved an $accu_y$ of 99.72%, while RFIRC-ODL, WFDLN, Alex-Net, Mobile-Net, Xception, and ResNet-50 approaches achieved 99.61%, 98%, 89.50%, 92.90%, 92.80%, and 94.51%, respectively. These results indicate the advanced efficiency of the proposed IWOADL-RFIGR method.

V. CONCLUSION

This study developed the innovative IWOADL-RFIGR method for retrieving and classifying retinal fundus images. In the first stage, the presented IWOADL-RFIGR method used the BF approach to preprocess the retinal images. For image retrieval, the IWOADL-RFIGR method used lightweight CNN based on scratch learning with Euclidean distance-based similarity measurement. Furthermore, the IWOADL-RFIGR method used IWOA with the LS-SVM method for image classification. The experimental validation of the proposed IWOADL-RFIGR method on the benchmark dataset exhibited better performance than other techniques. In the future, the proposed IWOADL-RFIGR method will be extended to the design of the deep instance segmentation process.

REFERENCES

[1] A. Imran, J. Li, Y. Pei, F. Akhtar, J.-J. Yang, and Y. Dang, "Automated identification of cataract severity using retinal fundus images," *Computer Methods in Biomechanics and Biomedical Engineering: Imaging & Visualization*, vol. 8, no. 6, pp. 691–698, Nov. 2020, https://doi.org/10.1080/21681163.2020.1806733.

[2] A. Shoukat, S. Akbar, S. A. E. Hassan, A. Rehman, and N. Ayesha, "An Automated Deep Learning Approach to Diagnose Glaucoma using Retinal Fundus Images," in *2021 International Conference on Frontiers of Information Technology (FIT)*, Islamabad, Pakistan, Sep. 2021, pp. 120–125, https://doi.org/10.1109/FIT53504.2021.00031.

[3] M. Mateen, J. Wen, Nasrullah, S. Song, and Z. Huang, "Fundus Image Classification Using VGG-19 Architecture with PCA and SVD," *Symmetry*, vol. 11, no. 1, Jan. 2019, https://doi.org/10.3390/sym11010001.

[4] M. Juneja, N. Thakur, S. Thakur, A. Uniyal, A. Wani, and P. Jindal, "GC-NET for classification of glaucoma in the retinal fundus image," *Machine Vision and Applications*, vol. 31, no. 5, Jun. 2020, Art. no. 38, https://doi.org/10.1007/s00138-020-01091-4.

[5] S. Goel *et al.*, "Deep Learning Approach for Stages of Severity Classification in Diabetic Retinopathy Using Color Fundus Retinal Images," *Mathematical Problems in Engineering*, vol. 2021, Nov. 2021, Art. no. 7627566, https://doi.org/10.1155/2021/7627566.

[6] D. R. Parashar and D. K. Agarwal, "SVM based Supervised Machine Learning Framework for Glaucoma Classification using Retinal Fundus Images," in *2021 10th IEEE International Conference on Communication Systems and Network Technologies (CSNT)*, Bhopal, India, Jun. 2021, pp. 660–663, https://doi.org/10.1109/CSNT51715.2021.9509708.

[7] J. K. P. S. Yadav and S. Yadav, "Computer-aided diagnosis of cataract severity using retinal fundus images and deep learning," *Computational Intelligence*, vol. 38, no. 4, pp. 1450–1473, 2022, https://doi.org/10.1111/coin.12518.

[8] K. Shankar, A. R. W. Sait, D. Gupta, S. K. Lakshmanaprabu, A. Khanna, and H. M. Pandey, "Automated detection and classification of fundus diabetic retinopathy images using synergic deep learning model," *Pattern Recognition Letters*, vol. 133, pp. 210–216, May 2020, https://doi.org/10.1016/j.patrec.2020.02.026.

[9] R. Poplin *et al.*, "Prediction of cardiovascular risk factors from retinal fundus photographs via deep learning," *Nature Biomedical Engineering*, vol. 2, no. 3, pp. 158–164, Mar. 2018, https://doi.org/10.1038/s41551-018-0195-0.

[10] S. Gupta, A. Panwar, S. Goel, A. Mittal, R. Nijhawan, and A. K. Singh, "Classification of Lesions in Retinal Fundus Images for Diabetic Retinopathy Using Transfer Learning," in *2019 International Conference on Information Technology (ICIT)*, Bhubaneswar, India, Sep. 2019, pp. 342–347, https://doi.org/10.1109/ICIT48102.2019.00067.

[11] D. D. Van, "Application of Advanced Deep Convolutional Neural Networks for the Recognition of Road Surface Anomalies," *Engineering, Technology & Applied Science Research*, vol. 13, no. 3, pp. 10765–10768, Jun. 2023, https://doi.org/10.48084/etasr.5890.

[12] A. Munshi, "Randomly-based Stepwise Multi-Level Distributed Medical Image Steganography," *Engineering, Technology & Applied Science Research*, vol. 13, no. 3, pp. 10922–10930, Jun. 2023, https://doi.org/10.48084/etasr.5935.

[13] M. M. H. Milu, M. A. Rahman, M. A. Rashid, A. Kuwana, and H. Kobayashi, "Improvement of Classification Accuracy of Four-Class Voluntary-Imagery fNIRS Signals using Convolutional Neural Networks," *Engineering, Technology & Applied Science Research*, vol. 13, no. 2, pp. 10425–10431, Apr. 2023, https://doi.org/10.48084/etasr.5703.

[14] A. Pal, M. R. Moorthy, and A. Shahina, "G-Eyenet: A Convolutional Autoencoding Classifier Framework for the Detection of Glaucoma from Retinal Fundus Images," in *2018 25th IEEE International Conference on Image Processing (ICIP)*, Athens, Greece, Jul. 2018, pp. 2775–2779, https://doi.org/10.1109/ICIP.2018.8451029.

[15] M. N. Bajwa *et al.*, "Two-stage framework for optic disc localization and glaucoma classification in retinal fundus images using deep learning," *BMC Medical Informatics and Decision Making*, vol. 19, no. 1, Jul. 2019, Art. no. 136, https://doi.org/10.1186/s12911-019-0842-8.

[16] R. Acharya and N. B. Puhan, "Long Short-Term Memory Model Based Microaneurysm Sequence Classification in Fundus Images," in *2022 IEEE International Conference on Signal Processing and Communications (SPCOM)*, Bangalore, India, Jul. 2022, pp. 1–5, https://doi.org/10.1109/SPCOM55316.2022.9840789.

[17] H. Yu, F. He, and Y. Pan, "A scalable region-based level set method using adaptive bilateral filter for noisy image segmentation," *Multimedia Tools and Applications*, vol. 79, no. 9, pp. 5743–5765, Mar. 2020, https://doi.org/10.1007/s11042-019-08493-1.

[18] N. Gour and P. Khanna, "Ocular diseases classification using a lightweight CNN and class weight balancing on OCT images," *Multimedia Tools and Applications*, vol. 81, no. 29, pp. 41765–41780, Dec. 2022, https://doi.org/10.1007/s11042-022-13617-1.

[19] R. M. A. Ikram, H.-L. Dai, A. A. Ewees, J. Shiri, O. Kisi, and M. Zounemat-Kermani, "Application of improved version of multi verse optimizer algorithm for modeling solar radiation," *Energy Reports*, vol. 8, pp. 12063–12080, Nov. 2022, https://doi.org/10.1016/j.egyr.2022.09.015.

[20] C. Shi *et al.*, "Bending Force of Hot Rolled Strip Based on Improved Whale Optimization Algorithm and Twinning Support Vector Machine," *Metals*, vol. 12, no. 10, Oct. 2022, Art. no. 1589, https://doi.org/10.3390/met12101589.

[21] "Diabetic Retinopathy Detection." https://kaggle.com/competitions/diabetic-retinopathy-detection.

[22] G. U. Nneji, J. Cai, J. Deng, H. N. Monday, M. A. Hossin, and S. Nahar, "Identification of Diabetic Retinopathy Using Weighted Fusion Deep Learning Based on Dual-Channel Fundus Scans," *Diagnostics*, vol. 12, no. 2, Feb. 2022, Art. no. 540, https://doi.org/10.3390/diagnostics12020540.